Phys. Status Solidi B **249,** No. 10, 1890–1896 (2012) / **DOI** 10.1002/pssb.201200398

Part of Special Issue
Phase-change memory: Science and applications

physica status solidi b
www.pss-b.com
basic solid state physics

Tetrahedral germanium in amorphous phase change materials: Exploring the isochemical scenario

Matthieu Micoulaut*[,1], Ali Kachmar[1], and Thibault Charpentier[2]

[1] Laboratoire de Physique Théorique de la Matière Condensée, Université Pierre et Marie Curie, Boite 121, 4 place Jussieu, 75252 Paris Cedex 05, France
[2] CEA IRAMIS Service Interdisciplinaire sur les Systèmes Moléculaires et Matériaux, UMR CEA/CNRS 3299, 91191 Gif-sur-Yvette, France

Received 20 June 2012, revised 2 August 2012, accepted 2 August 2012
Published online 31 August 2012

Dedicated to Stanford R. Ovshinsky on the occasion of his 90th birthday

Keywords molecular dynamics simulations, phase change materials, structure, supercooled liquids

* Corresponding author: e-mail mmi@lptl.jussieu.fr, Phone: +33-1-44277240, Fax: +33-1-44275100

The structural, vibrational, and electronic properties of low-temperature supercooled $GeTe_4$ are studied using density functional theory (DFT). Two models have been considered: an ordinary melt-quenched system containing a majority of defect-octahedral germanium atoms, and a relaxed one obtained from a quenched $SiTe_4$ rescaled structure which contains mostly tetrahedral germanium, while leaving the Te environment preserved. The tetrahedral system exhibits an increased agreement with the experimental structure factor $S(k)$, the pair distribution function $g(r)$, and the infrared absorption spectrum. It is suggested that the fraction of tetrahedral Ge must be higher as usually believed. In addition, we provide the calculation of the ^{125}Te wideline NMR spectra. While the latter do not agree with recent experimental findings, both systems exhibit important significant differences in the widths of the computed spectra. These exploratory calculations clearly show that NMR will be an interesting probe that deserves further investigations for the experimental determination of the local geometry.

1 Introduction It is the great merit of Stanford Ovshinsky that, happily accumulating experiments on electrical switching in the late 1960s, he could propose a revolutionary mechanism [1] for data storage from phase change materials (PCMs) which are now at the heart of the multi-billion world-wide industry of computer memories. Given the time needed to transform his first laboratory device into a routinely used 100 Go BlueRay disk, nearly 40 years, the successful story of Ovshinsky's invention not only brings us back to other modern creations of humankind. It also illustrates at the very best level the large time interval needed to accept scientifically a breakthrough in fundamental science, and to design applications from the discovery prior to its potential large-scale industrial production. On this special occasion of Stan's 90th birthday, it is therefore a great pleasure to dedicate this article to him.

At the early stage of PCM history, amorphous telluride systems have been identified as an interesting class of materials with phase-change properties. In fact, they have low melting and glass transition temperatures, and an important optical and electrical contrast between the crystalline and amorphous phase [2]. Another well-documented application, independent of PCMs, deals with the fact that amorphous tellurides display an exceptionally large optical transmittance domain which makes their use as waveguides for infrared integrated optics extremely interesting [3].

Whatever the considered complex ternary or quaternary telluride, the base material used for the optimization of functionalities is the Ge–Te binary which has received a huge attention, and is rather well documented in the literature [2]. Focus on the phase change compositions GeTe and $GeTe_6$, and particularly on structure [4–6], has somewhat overshadowed other interesting properties which can exhibit a certain number of remarkable anomalies with changing temperature or composition [7]. The latter allows also to tune the connectivity of the amorphous network so that a flexible

to rigid transition is expected in tellurides [8] similarly to Ge–Se glasses [9].

When applied to telluride systems, FPMD usually overestimates the bond lengths, among which the Ge–Te one. This leads to a disagreement between theory and experiment (*e.g.*, neutron diffraction) in the reproduction [5, 6] of the pair distribution function g(r), and especially the first peak measured at 2.60 Å corresponding to the Ge–Te bond distance d^1_{GeTe} [10], to be compared with the calculated value [11] of 2.68 Å in $GeTe_6$.

One should furthermore remark that the local geometry strongly influences the Ge–Te bond length. It has been indeed suggested that the fourfold germanium was existing under two types of local structures: a tetrahedral one and a defect octahedral one with two vacancies. Tetrahedral Ge leads to four very close neighbors around 2.8 Å whereas the dominant defect-octahedral geometry has bonds which are much longer (3.13 Å) [4, 6, 12, 13]. In this respect, it is tempting to investigate the effect of an increased fraction of tetrahedral Ge on the structural observables. The picture of a tetrahedral Ge in amorphous tellurides, responsable for phase-change properties, has been first proposed by Kolobov et al. [14] on the basis of X-ray fine absorption, but several experimental and numerical studies have proposed an alternative picture consisting of a structure made of a majority of defect-octahedral Ge [12, 13, 15]. Simulated Ge–Te systems obviously contain tetrahedral Ge. The fraction can be estimated from the charge localization through a Wannier function analysis [16]. Also, a calculation of the vibrational properties has shown that there is a specific signature of tetrahedral Ge in the Raman spectra [15], and that their presence can be merely quantified through an orientational order parameter [13].

In the present contribution, we are guided by the same motivation as the one sketched in many of the aforementioned references, *i.e.*, we ask the question of how a standard DFT approach which is known to produce a structure disagreeing with experiments, the usual bond distance problem, can be modified in order to improve accuracy. While acknowledging the RMC refinement [17] as a promising pathway, an alternative strategy can be proposed. Here, we investigate the structural, electronic, and vibrational properties of a supercooled $GeTe_4$ having a majority of tetrahedral germanium. Results are compared with a benchmark $GeTe_4$ obtained from a usual melt-quenched liquid using FPMD. The latter contains a majority of defect-octahedral Ge as in previous studies for different compositions [4, 6, 12, 17]. The $GeTe_4$ compound itself has not received much attention although it has been shown recently that films [18] have a higher crystallization temperature and a lower melting temperature when compared with GeTe and the ternary $Ge_2Sb_2Te_5$, indicating that this compound may also be a competitive candidate for memory applications.

How can one build such $GeTe_4$ tetrahedral models? We consider an isochemical compound, that is a melt-quenched tetrahedral $SiTe_4$, which is used as starting configuration for a low temperature $GeTe_4$. Such a strategy has been used in the past to investigate, *e.g.*, germania based on models of the isochemical silica [19]. It has been also used recently [20] in order to study an ideal amorphous $Ge_2Sb_2Te_5$ using the isochemical $Si_2As_2Se_5$. However, in contrast with the latter, in the present contribution we have substituted only one type of atom in order to probe the sensitivity on the local Ge structure, while leaving the Te environment preserved.

Inspection of the pair distribution functions (pdfs, Fig. 1) obtained from FPMD (see Methods section below) shows indeed that $SiTe_4$ and $GeTe_4$ mostly differ in the environment involving the Group IV atom, while the Te–Te correlation appears to be nearly unchanged. The Si–Te pdf displays a very sharp peak indicative of a well-defined local geometry as in other archetypal tetrahedral liquids such as $GeSe_2$ [23], as also detected from the Te–Si–Te bond angle distribution (inset B of Fig. 1). The latter displays indeed the

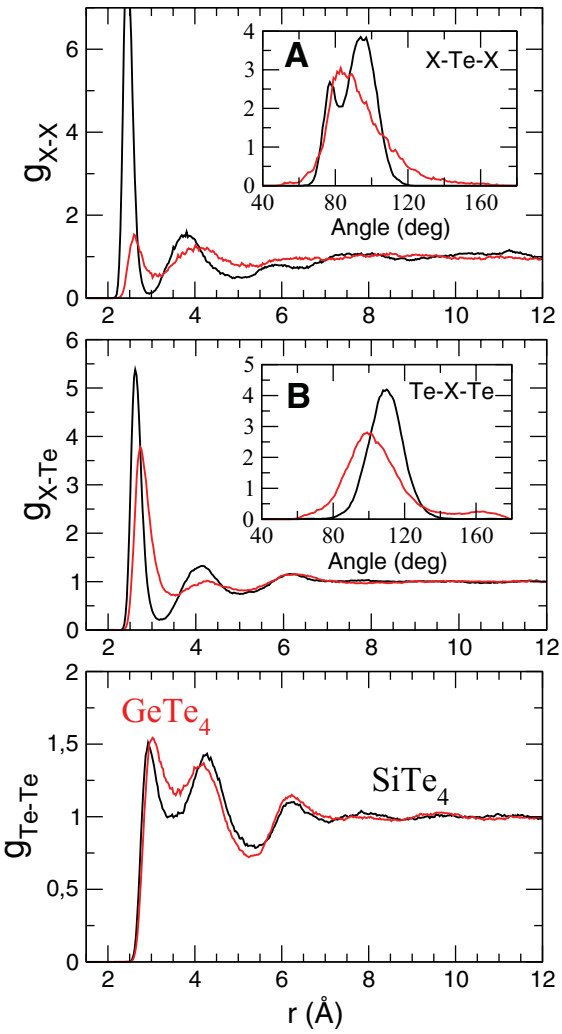

Figure 1 (online color at: www.pss-b.com) Pair distribution functions at 450 K in $GeTe_4$ (red) and $SiTe_4$ (black). The insert A and B shows the bond angle distributions X–Te–X and Te–X–Te (X = Ge, Si), respectively.

usual tetrahedral angle (109°) whereas contributions at 90° and 180° for the $GeTe_4$ clearly indicate an octahedral environment. On the contrary, the pdfs of $GeTe_4$ are found to be similar to those obtained for a close composition [5]. The difference in structure can be qualitatively explained from the crystalline counterparts. The Si–Te system crystallizes in a trigonal Si_2Te_3 structure which is tetrahedral [21] and contains homopolar Si–Si bonds, whereas the Ge–Te crystalline form is found at 50% Ge and is made of two embedded rocksalt-type sub-lattices [22] containing either Ge or Te with no Ge–Ge bonds. The corresponding liquid and amorphous local structures are therefore reminiscent of the crystals, and may also provide some very basic understanding on the large difference between homopolar distributions Ge–Ge and Si–Si.

Here it is shown from FPMD that simulated structural properties of a tetrahedral $GeTe_4$ model leads to an increased agreement of the total neutron structure factor, the pair distribution function, and the infrared absorption spectrum. An analysis of the structure, bond distances, and coordination numbers is provided. The tetrahedral system also shows an increased gap at the Fermi energy. Finally, we compute the NMR spectra for both systems which shows a much broader distribution for the octahedral $GeTe_4$.

2 Computational methods FPMD simulations have been performed at constant volume on a system containing 200 (160 Ge/Si and 40 Te) atoms positioned in a periodically repeated cubic cell whose size followed exactly the experimental density of the liquid [7, 24] at the desired temperatures. The electronic structure was described within density functional theory (DFT) and evolved self-consistently during the motion [25]. A generalized gradient approximation was used, based on the exchange-correlation energy obtained by Perdew, Burke, and Ernzerhof [25]. Valence electrons have been treated explicitly, in conjunction with Trouiller–Martins norm conserving pseudopotentials. The wave functions have been expanded at the Γ point of the supercell on a plane wave basis set with an energy cutoff $E_c = 20$ Ry. In the FPMD simulation, a fictitious electron mass of 200 a.u. (*i.e.*, in units of $m_e a_0^2$ where m_e is the electron mass and a_0 is the Bohr radius), and a time step of $\Delta t = 0.12$ fs have been used to integrate the equations of motion. Temperature control has been implemented for both the ionic and electronic degrees of freedom by using Nosé–Hoover thermostats [25].

The two systems ($GeTe_4$ and $SiTe_4$) have been cooled from 2000 K (starting random configuration) down to 450 K (obtained structure in Fig. 1) at an approximate cooling rate of 10 K ps^{-1}, corresponding to temperature intervals of $\Delta T = 200$ K at which trajectories of about 25 ps have been accumulated. On the overall, this corresponds to a cooling time of about 250 ps. At 450 K, the $SiTe_4$ atomic positions (properly rescaled) have been used as starting configuration for a $GeTe_4$ system which has been relaxed at 450 K over 25 ps. Ultimately, the system had a total energy which was lower by 0.088 eV atom^{-1} as compared to the melt-quenched $GeTe_4$. Details on the structure of liquid and amorphous $SiTe_4$ will be reported elsewhere. In the following, we compare various properties calculated from this relaxed structure (termed *Tetra* hereafter) with those obtained for the ordinary melt-quenched $GeTe_4$ (termed *Octa* hereafter).

DFT NMR calculations were carried out with Quantum Espresso [26] using the Gauge-Including Projected Augmented Wave (GIPAW) method [27] with a single Baldereschi point (and the same DFT functional and norm-conserving pseudopotentials employed during the melt-quench procedure). GIPAW outputs were processed using the fpNMR software in order to perform the simulations of the NMR spectra, as described in Ref. [28]. The calculations have been performed using the 25 ps relaxed configurations. Only ^{125}Te ($I = 1/2$) wideline NMR results are reported, considering that experimental data have been reported recently [29]. The calculated ^{125}Te NMR chemical shifts are reported with respect to crystalline GeTe (calculated isotropic chemical was fixed at −4000 ppm), following standard procedure described in Ref. [28].

3 Results In Fig. 2, we show the comparison between the calculated structure factor $S_T(k)$ of the two $GeTe_4$ systems (*Tetra* and *Octa*) and the experimental counterpart [10, 30]. At a global level, the *Tetra* system leads to a clear improvement in the shape of $S_T(k)$ for all wavevectors. We find not only an improved agreement in the low wavevector region ($k \sim 1$ Å^{-1}), but also for all the main peaks located at 2.1, 3.3, and 5.1 Å^{-1}, the main peak at 2.1 Å^{-1} being, in fact, overestimated in the *Octa* system. Finally, one can notice that the width of the peaks is also substantially improved when one increases the fraction of tetrahedral Ge. We acknowledge the improved reproduction of the high-k tail of the secondary peak at 3.3 Å^{-1}, but also an increased accuracy for the region between 3.8 and 5 Å^{-1}. For the high wavector region, an increased agreement is also obtained, under-

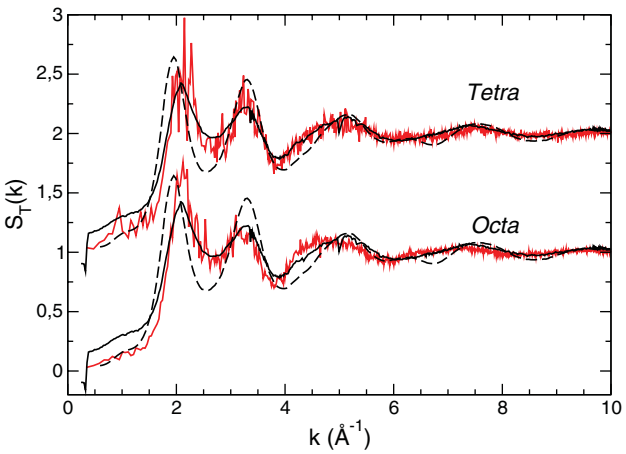

Figure 2 (online color at: www.pss-b.com) Total neutron structure factor $S_T(k)$ of *Octa*- or *Tetra*-$GeTe_4$ (red curves), compared to available experimental data in the liquid (700 K, solid line [30]) and in the amorphous phase (broken line) [10].

scoring that the local structure may also be improved, as discussed below.

Figure 2 represents the first piece of evidence that an increased fraction of tetrahedral germanium concurs to improve the long-range behavior, while the changes induced in the short-range range behavior are smaller. An analysis of the Faber–Ziman partial structure factors (not shown) indicates that most changes are found in $S_{GeTe}(k)$, while the two other partials $S_{GeGe}(k)$ and $S_{TeTe}(k)$ are almost identical. In particular, the difference observed in the region 3.8–5 Å^{-1} between the *Tetra* and the *Octa* system (Fig. 2) are also recovered in $S_{GeTe}(k)$ which signals that the disagreement between the structure of an *Octa* system and experimental data at this lengthscale arises from the Ge–Te correlations.

The total pair distribution function of the *Tetra* and *Octa* system are shown in Fig. 3, and compared to experimental data [10, 30]. First, it should be remarked that the *Tetra* system leads, in fact, to shorter bonds as compared to the *Octa* $GeTe_4$, a result is not only a consequence of the initial Si–Si and Si–Te distances (Fig. 1) which are shorter (and the box size of $SiTe_4$ which is larger), but also a result of the presence of the majority of tetrahedral motifs which are found to display shorter Ge–Te bond distances than the Ge–Te in defective octahedra obtained in melt-quenched amorphous phases [13]. The low-*r* side of the principal peak (PP) located at 2.72 Å [10, 30] is better reproduced and arises from several contributions: homopolar Ge–Ge and Te–Te bonds found at $d^1_{GeGe} = 2.45$ Å and $d^1_{TeTe} = 2.93$Å, respectively, and heteropolar Ge–Te bonds calculated at $d^1_{GeTe} = 2.64$ Å (Table 1). The overestimate of $d^1_{TeTe} = 2.93$ Å is one of the salient features of the PBE pseudopotential for Te [32] which leads to a contribution on the high-r side of the PP. We notice that the obtained bond distances are close to those obtained from a DFT simulation of as-deposited GST ($d^1_{GeTe} = 2.69$ Å) where tetrahedral Ge dominates [33]. The system obtained in a tetrahedral geometry is found to display an increased structuration, reminiscent of the initial $SiTe_4$ system, as seen from the more pronounced minimum

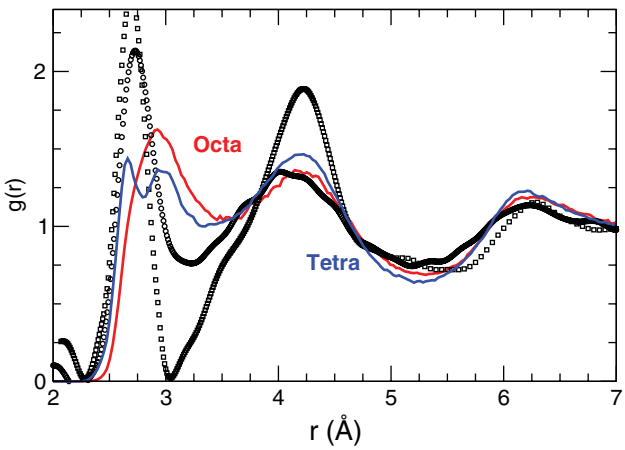

Figure 3 (online color at: www.pss-b.com) Total pair distribution function $g(r)$ of Octa- (red) or Tetra-$GeTe_4$ (blue), compared to experimental results (700 K (circles) [30]; 300 K (squares) [10]).

Table 1 Calculated position (in Å, ±0.03 Å) of the first peak d^1_{ij} (bond distance) and second peak d^2_{ij} of the pdfs in $GeTe_4$, having a majority of tetrahedral or octahedral Ge.

	octa	*tetra*	exp.
d^1_{GeGe}	2.56	2.45	
d^2_{GeGe}	3.85	3.72	
d^1_{GeTe}	2.74	2.64	2.62 [31]
			2.63 [10]
d^2_{GeTe}	4.38	4.14	
d^1_{TeTe}	3.05	2.93	2.82 [31]
d^2_{TeTe}	4.14	3.98	

found at 3.4 Å. In addition, simulation shows that Ge has a well-defined range of bond-distances and a gap before non-bonding distances, a situation that is clearly met in the observed experimental pair distribution function [10] in Te-rich Ge–Te binary glasses (here at 3 Å, see Fig. 3).

From the partials, we extract the corresponding coordination numbers (at the minimum r_m of the pdfs) which are equal to $n_{GeGe}(r_m = 2.87\,\text{Å}) = 0.32$, $n_{TeGe}(r_m = 3.40\,\text{Å}) = 1.12$ and $n_{GeTe} = 4.48$, and $n_{TeTe}(r_m = 3.51\,\text{Å}) = 3.01$ for the *Octa* system. This leads to coordination numbers equal to $n_{Ge} = 4.8$ 4.8 and $n_{Te} = 4.13$, a result which exceeds by far what is expected from experiments [31, 35]. Note that usually an arbitrary (lower) cut-off distance is chosen for all pairs (typically 3.2 Å) which brings results closer [17] to experimental findings. For the *Tetra* system, one obtains $n_{GeGe}(r_m = 2.86\,\text{Å}) = 0.85$, $n_{TeGe}(r_m = 3.14\,\text{Å}) = 0.80$ and $n_{GeTe} = 3.2$, and $n_{TeTe}(r_m = 3.27\,\text{Å}) = 2.08$ which leads to $n_{Ge} = 4.05$ and $n_{Te} = 2.88$, in closer agreement with results from other MD studies but different from those obtained from X-ray absorption ($n_{Te} = 2.0 \pm 0.1$ [31]).

The study of the local topology of both systems (Table 2) shows that the *Tetra* system contains a larger amount of fourfold Ge atoms (87%) while defect Ge^{III} and Ge^{V} appear in higher fractions in a melt quenched $GeTe_4$, leaving only 58% of Ge^{IV}. An increased fraction of twofold Te atoms is also obtained, consistently with the estimation from the pair distribution functions performed above.

In addition, we compute the departure from pure chemical order. For a perfect chemical network, all Ge

Table 2 Nearest neighbor analysis and average number of neighbors of Ge (3,4,5) and Te (1, 2, 3) at 3 Å (in %), together with an estimate of the departure from a chemically ordered network (AA, AB, BB, see text for details). Comparison with $GeSe_4$ [34].

		1	2	3	4	5	AA	AB	BB
octa	Ge		5	25	58	12	24	50	26
	Te	34	54	12					
tetra	Ge			5	87	8	27	50	23
	Te	31	60	9					
$GeSe_4$							26	47	23

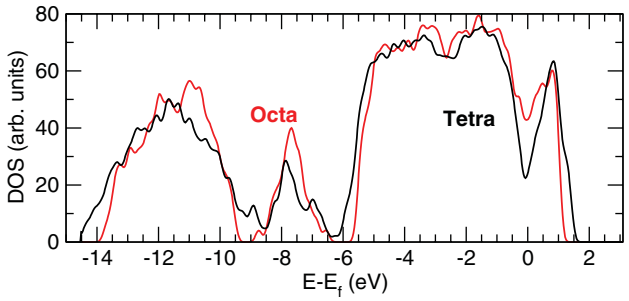

Figure 4 (online color at: www.pss-b.com) Electronic density of states of the *Octa* (red) or *Tetra* (black) $GeTe_4$.

atoms are indeed connected by Te_2 dimers. We concentrate on the twofold atoms only (54% in *Octa* and 60% in the *Tetra*) and compute for these the probability of having either two Te neighbors (BB motif, at least Ge–Te–Te–Te–Ge, see Ref. [34]), either one Ge and one Te neighbor (AB motif, Ge–Te–Te–Ge) and two Ge neighbors (BB motif, Ge–Te–Ge, representative of the $GeTe_2$ stochiometry). In a chemically ordered system, one expects the fractions of AA, BB, and AB connections to be 0, 0, and 100%, respectively. Table 2 shows results for both *Tetra* and *Octa* systems which display nearly the same departure from a chemically ordered network with a close fraction of 25:50:25. Furthermore, one sees that these fractions are also close to those found for lighter chalcogenides such as $GeSe_4$ [34]. One therefore concludes that the connectivity of $GeTe_4$ involving the twofold Te atoms resembles very much to the one found in the selenide analogue, this conclusion being valid for both models.

4 Electronic structure Figure 4 shows the electronic density of states (EDOS) of the *Tetra* and *Octa* systems. While the global EDOS profile remains the same with two s-bands between −14 and −6.2 eV, well separated from the valence p-band structure, one finds an increased pseudo-gap at the Fermi energy in the *Tetra* system. The latter shows in fact a marked minimum which is much more pronounced as compared to the *Octa* system. The width of this pseudo-gap (determined from the EDOS decrease to the minimum at the Fermi energy) is found to be 0.83 and 0.89 eV for the *Octa* and the *Tetra* system, respectively, to be compared to the experimental value of 0.86–093 eV measured in amorphous $GeTe_4$ [36].

5 Infrared spectra An additional means that can be used to discriminate between the *Octa* and the *Tetra* model is provided by the calculation of the infrared vibrational properties. During the DFT calculation, the total dipole moment $M(t)$ can be directly calculated [37] and contributes via the Fourier transform of the dipole–dipole autocorrelation function to the IR absorption spectrum using the maximum entropy inversion method [38]:

$$\alpha(\omega) = \frac{4\pi \tanh(\beta\hbar\omega/2)}{3\hbar c V n(\omega)} \int_0^\infty e^{-i\omega t} \langle M(t)M(0)\rangle dt, \quad (1)$$

where V is the volume, $\beta = 1/k_B T$, and $n(\omega)$ the refractive index. Figure 5 shows the computed IR spectra $\alpha(\omega)n(\omega)$ for both systems, compared to experimental data from Maurugeon et al. [39]. Clearly, the *Tetra* model reproduces the main absorption band found at 780 cm^{-1}, whereas it is completely absent for the *Octa* system which shows a main peak at a somewhat higher frequency (1081 cm^{-1}), and does not show any marked absorption frequency at the experimentally observed one. A vibrational analysis of an isolated $GeTe_{4/2}$ tetrahedron shows that the low frequencies (contributions at $\omega = 112$, 150, and 170 cm^{-1}) are associated with symetric and antisymetric bending, and symetric stretching Ge–Te modes, respectively. The present results validate from the vibrational analysis the possibility of an increased fraction of tetrahedral germanium in $GeTe_4$. However, one should keep in mind that the reproduction of such spectra is highly model sensitive [40].

6 ^{125}Te wideline NMR spectra We finally present a first NMR calculation of the *Tetra* and *Octa* $GeTe_4$. On the one hand, ^{125}Te NMR has been recently clearly established as a promising technique to study the short-range order in tellurides [29, 31, 41]. One the other hand, calculations of NMR interactions in solids with the GIPAW method are now well established [42]. The combination of both approaches (now generally referred to as first-principles NMR, fpNMR) offer therefore unique novel opportunities to provide new insights into the structure of these materials. Detailed fpNMR analysis of the present models is out of the scope of the present work, but we present preliminary results showing how the two studied models differ in their *NMR spectral signature*.

Although it has been found that both *Octa* and *Tetra* systems were displaying to some extent similar structural correlations through the $g(r)$ or $S(k)$ functions, it appears clearly from Fig. 6 that NMR is able to discriminate between

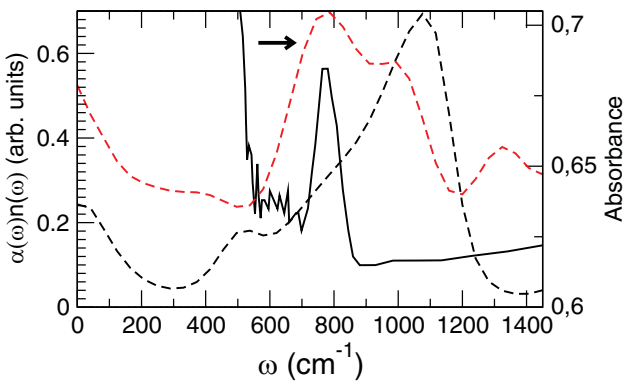

Figure 5 (online color at: www.pss-b.com) Computed infrared absorption (IR) spectra (rescaled) of $GeTe_4$ for the *Tetra* (broken red curve) and *Octa* model (broken black curve), compared to experimental IR absorbance data (solid line, right axis) [39]. Note that the steep decrease in the experimental spectrum at ∼550 cm^{-1} arises from a strong increase of the measured transmission coefficient T, T being nearly zero for $\omega < 500$ cm^{-1}.

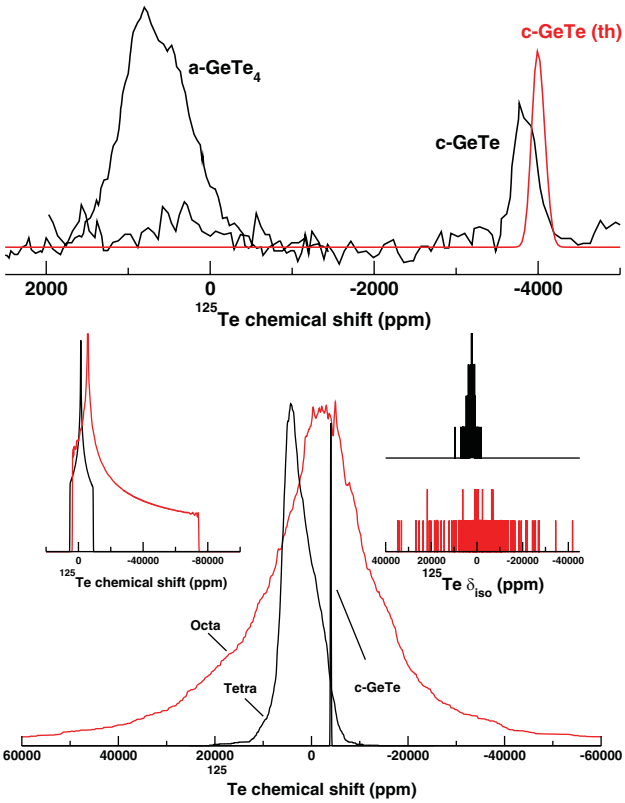

Figure 6 (online color at: www.pss-b.com) Top: Simulated ^{125}Te wideline NMR spectra (red curve) of c-GeTe compared to the corresponding experimental analogue (black), together with the experimental spectra of amorphous $GeTe_4$ [29]. Bottom: Simulated ^{125}Te wideline NMR spectra of the *Octa* (red) and *Tetra* system (black), and crystalline GeTe (same as top). Left inset shows typical wideline NMR lineshape for a single site, as induced by chemical shift anistoropy (CSA). Right inset shows the distribution of isotropic chemical shift for both models.

the two dominant environments, tetrahedral or octahedral. Indeed, while the anisotropy of the chemical shifts appears to be substantially overestimated for both, with a peak maximum at 4100 and −2000 ppm for the *Tetra* and *Octa* systems, respectively (to be compared with the one found experimentally at 800 ppm [29]), one finds that the dispersion of the chemical shift is much more pronounced in the *Octa* system. In wideline NMR, width of the lines is both reflective of the anisotropy of the chemical shift (CSA) and dispersion of the isotropic chemical shift δ_{iso} and CSA values, as induced by the structural disorder (insets of Fig. 6). From a NMR point of view, the *Tetra* model seems to be more ordered and somewhat in better agreement with the experimental data. Because of the contribution of distribution of both δ_{iso} and CSA, use of more advanced techniques in future as described in Ref. [43] will clearly provide better insight into experimental data.

Nonetheless, the significant discrepancy between simulated and experimental data deserves some comment. The origin of this important difference cannot only arise from temperature effects (here 450 K) which usually broaden the NMR peaks [42]. Given the high sensitivity of NMR to fine structural variations (such as bond angle distribution and interatomic distances), this could also simply result from the structural models themselves. It would therefore be interesting to compare the method with other reference composition including, *e.g.*, other elements such as As or Sb [29]. Work in this direction is in progress.

Another possible origin is the fact that we compute only the chemical shift interactions. If both systems exhibit some metallic properties (as shown from the presence of a pseudogap in Fig. 4), then Knight shift contribution would have to be incorporated (but presently no code implemented in this calculations).

7 Summary and conclusions In the present contribution, we have investigated some of the structural, vibrational, and electronic properties of two possible models of $GeTe_4$: a system with a majority of octahedral Ge obtained after a standard melt-quench, and a $GeTe_4$ generated from a relaxation of the isochemical $SiTe_4$ containing only tetrahedra. Results show that for the latter an increased agreement on structure and IR absorption is obtained when compared to experimental data. The local topology shows an increased fraction of defect coordinations (three and fivefold) in the octahedral $GeTe_4$ whereas the number of twofold Te is increased in the $SiTe_4$ based system. On the contrary, the connectedness of the network does not seem to be sensitive to the local geometry as departure from chemical order (*i.e.*, 100% Ge–Te–Te–Ge) is found to be very similar, and also close to the parent system $GeSe_4$. An preliminary analysis of the NMR spectra shows that an increased computational effort is clearly needed to simulate properly the experimental spectra, although the tetrahedral system already displays the standard features of the experimental NMR spectrum. These results indicate that NMR is a promising technique for the investigation of PCMs [41].

On a more general ground, the present numerical study shows, again, that an amorphous system obtained from a Molecular Dynamics simulation represents only an ultrafast quenched high-temperature liquid. In covalent chalcogenides, it is known that such liquids contain a large number of mis-coordinated atoms and defect geometries [44] which are frozen down to low temperature due, in part, to the minuscule relaxation. In the covalent or semi-metallic tellurides, such effects seem to be even enhanced. These are well-known flaws of the technique, and one is therefore left with alternative strategies for the investigation of systems having no rigid geometries such as the one induced by sp^3 hybridization.

Acknowledgements The authors thank C. Bichara, P. Boolchand, M.-V. Coulet, C. Massobrio, A. Piarristeguy, A. Pradel for useful discussions. They are greatly indebted to Dr. Mauro Boero for technical help and advise. Palet and Opera are also gratefully acknowledged. This work has been supported by ANR-2011-BS08-012-01 project TEAM. This work was partially granted access to HPC

resources of CCRT under the allocation 2012-t2012096303 made by GENCI (Grand Equipement National de Calcul Intensif).

References

[1] S. Ovshinsky, Phys. Rev. Lett. **21**, 1450 (1968).
[2] S. Raoux and M. Wuttig (eds.), Phase Change Materials and Applications (Springer, Berlin, 2008).
[3] A. A. Wilhelm, C. Boussard-Plédel, Q. Coulombier, J. Lucas, B. Bureau, and P. Lucas, Adv. Mater. **19**, 3796 (2007).
[4] J. Akola and R. O. Jones, Phys. Rev. B **76**, 235201 (2007).
[5] C. Bichara, M. Johnson, and J.-Y. Raty, Phys. Rev. Lett. **95**, 267801 (2005).
[6] J. Akola and R. O. Jones, Phys. Rev. Lett. **100**, 205502 (2008).
[7] Y. Tsuchiya, J. Phys. Soc. Jpn. **57**, 3851 (1988).
[8] M. Micoulaut, C. Otjacques, J.-Y. Raty, and C. Bichara, Phys. Rev. B **81**, 174206 (2010).
[9] M. Micoulaut and J. C. Phillips, Phys. Rev. B **67**, 104204 (2003).
[10] I. Kaban, Th. Halm, W. Hoyer, P. Jòvari, and J. Neuefeind, J. Non-Cryst. Solids **326/327**, 120 (2003).
[11] C. Bergman, C. Bichara, J.-P. Gaspard, and Y. Tsuchiya, Phys. Rev. B **67**, 104202 (2003).
[12] J.-Y. Raty, C. Otjacques, J. P. Gaspard, and C. Bichara, Solid State Sci. **12**, 193 (2010).
[13] S. Caravati, M. Bernasconi, T. D. Kuehne, M. Krack, and M. Parrinello, Appl. Phys. Lett. **91**, 171906 (2007).
[14] A. V. Kolobov, P. Fons, A. I. Frenkel, A. L. Ankudinov, J. Tominaga, and T. Uruga, Nature Mater. **3**, 703 (2004).
[15] R. Mazzarello, S. Caravati, S. Angioletti-Uberti, M. Bernasconi, and P. Parrinello, Phys. Rev. Lett. **107**, 039902 (2010).
[16] G. C. Sosso, S. Caravati, R. Mazzarello, and M. Bernasconi, Phys. Rev. B **83**, 134201 (2011).
[17] J. Kalikka, J. Akola, R. O. Jones, S. Kohara, and T. Usuki, J. Phys.: Condens Matter **24**, 015802 (2012).
[18] H. Jiang, K. Guo, H. Xu, Y. Xia, K. Jiang, F. Tang, J. Yin, and Z. Liu, J. Appl. Phys. **109**, 066104 (2011).
[19] D. L. Price, M.-L. Saboungi, and A. C. Barnes, Phys. Rev. Lett. **81**, 3207 (1998).
[20] E. Cho, J. Im, C. Park, W. J. Son, D. H. Kim, H. Horii, J. Ihm, and S. Han, J. Phys.: Condens Matter **22**, 205504 (2010).
[21] K. Ploog, W. Stetter, A. Nowitzki, and E. Schnherr, Mater. Res. Bull. **11**, 1147 (1976).
[22] S. Kohara, K. Kato, S. Kimura, H. Tanaka, T. Usuki, K. Suzuya, H. Tanaka, Y. Moritomo, T. Matsunaga, N. Yamada, Y. Tanaka, H. Suematsu, and M. Takata, Appl. Phys. Lett. **89**, 201910 (2006).
[23] C. Massobrio, P. S. Salmon, and M. Micoulaut, Solid State Sci. **12**, 199 (2010).
[24] Y. Tsuchiya, J. Non-Cryst. Solids **136**, 37 (1991).
[25] D. Marx and J. Hutter, Ab Initio Molecular Dynamics: Theory and Implementation, in: Modern Methods and Algorithms of Quantum Chemistry, edited by J. Grotendorst (NIC, FZ Jülich, 2000).
[26] P. Giannozzi, S. Baroni, N. Bonini, M. Calandra, R. Car, C. Cavazzoni, D. Ceresoli, G. L. Chiarotti, M. Cococcioni, I. Dabo, A. Dal Corso, S. de Gironcoli, S. Fabris, G. Fratesi, R. Gebauer, U. Gerstmann, C. Gougoussis, A. Kokalj, M. Lazzeri, L. Martin-Samos, N. Marzari, F. Mauri, R. Mazzarello, S. Paolini, A. Pasquarello, L. Paulatto, C. Sbraccia, S. Scandolo, G. Sclauzero, A. P. Seitsonen, A. Smogunov, P. Umari, and R. M. Wentzcovitch, J. Phys.: Condens. Matter **21**, 395502 (2009).
[27] C. J. Pickard and F. Mauri, Phys. Rev. B **63**, 245101 (2001).
[28] A. Pedone, T. Charpentier, and M. C. Menziani, Phys. Chem. Chem. Phys. **12**, 6054 (2010).
[29] T. G. Edwards, E. L. Gjersing, S. Sen, S. C. Currie, and B. G. Aitken, J. Non-Cryst. Solids **357**, 3036 (2011).
[30] M. Micoulaut, M.-V. Coulet, A. Piarristeguy, C. Bichara, A. Pradel, and J.-Y. Raty, submitted (2012).
[31] S. Sen, S. Joshi, B. G. Aitken, and S. Khalid, J. Non-Cryst. Solids **354**, 4620 (2008).
[32] J. Akola and R. O. Jones, J. Phys.: Condens. Matter **20**, 465103 (2008).
[33] J. Akola, J. Larrucea, and R. O. Jones, Phys. Rev. B **83**, 094113 (2011).
[34] C. Massobrio, M. Celino, P. S. Salmon, R. A. Martin, M. Micoulaut, and A. Pasquarello, Phys. Rev. B **79**, 174201 (2009).
[35] D. A. Baker, M. A. Paessler, G. Lucovsky, S. C. Agarwal, and P. C. Taylor, Phys. Rev. Lett. **96**, 255501 (2006).
[36] P. Petkov, M. Wuttig, P. Ilchev, and T. Petkova, J. Optoelectron. Adv. Mater. **5**, 1101 (2003).
[37] P. L. Silvestrelli, M. Bernasconi, and M. Parinello, Chem. Phys. Lett. **277**, 478 (1997).
[38] R. N. Silver, D. S. Silvia, and J. E. Gubernatis, Phys. Rev. B **41**, 2380 (1990).
[39] S. Maurugeon, B. Bureau, C. Boussard-Plédel, A. J. Faber, X. H. Zhang, W. Geliesen, and J. Lucas, J. Non-Cryst. Solids **355**, 2074 (2009).
[40] L. Giacomazzi, C. Massobrio, and A. Pasquarello, Phys. Rev. B **75**, 174207 (2007).
[41] S. Sen, T. G. Edwards, J.-Y. Cho, and Y.-C. Yoo, Phys. Rev. Lett. **108**, 195506 (2012).
[42] T. Charpentier, Solid State Nucl. Magn. Res. **40**, 1 (2011).
[43] Y.-Y. Hu, E. M. Levin, and K. Schmidt-Rohr, J. Am. Ceram. Soc. **131**, 8390 (2009).
[44] M. Micoulaut, R. Vuilleumier, and C. Massobrio, Phys. Rev. B **79**, 214205 (2009).

